2009-32-0185 / 20097185

Combustion System Development and Analysis of a Downsized Highly Turbocharged PFI Small Engine

William P. Attard, Elisa Toulson, Ferenc Hamori and Harry C. Watson
University of Melbourne, Australia

ABSTRACT

This paper provides some insight into the future direction for developing smaller capacity downsized engines, which will be needed to meet tight CO_2 targets and the world's future powertrain requirements. This paper focuses on the combustion system development and combustion analysis results for a downsized 0.43 liter highly turbocharged engine. The inline two cylinder engine used in experiments was specifically designed and constructed to enable 25 bar BMEP. Producing this specific output is one way forward for future passenger vehicle powertrains, enabling in excess of 50% swept capacity reduction whilst maintaining comparable vehicle performance.

Previous experiments and analysis have found that the extent to which larger engines can be downsized while still maintaining equal performance is combustion limited. Hence, small engine combustion is explored over a number of parametric studies, including a range of manifold absolute pressures up to 270 kPa, engine speeds exceeding 10,000 rev/min and compression ratios ranging from 9 to 13. Experimental results indicate that small engine combustion hurdles can be overcome to reliably extend the specific output to 25 bar BMEP. This is believed to be the highest recorded specific output for a non-intercooled small spark ignition PFI engine operating on pump gasoline. However, the boosted combustion effects illustrate that the thermal efficiency is highly dependent on the combustion efficiency, which deteriorates rapidly if uncontrolled combustion, specifically knock in the end-gas region is encountered. However, with this combustion system design strategy, potential drive cycle fuel consumption improvements in excess of 20% are still achievable.

INTRODUCTION

Growing concerns about interruption to oil supply and oil shortages have led to escalating and unstable global oil prices. In addition, increased public acceptance of the global warming problem has prompted car manufacturers to agree to carbon emission targets in many regions including most recently, the United States. Other legislating bodies are sure to follow this lead with increasingly stringent targets. As a result of these issues, spark ignition engines in their current form will need significant improvements to meet future requirements. One technically feasible option is smaller capacity downsized engines (~70 mm bore diameter) which operate at a higher manifold pressure for a given road load (part load pumping loss benefits) when compared to larger capacity counterparts. These small downsized engines with enhanced power could be used in the near term to reduce both carbon emissions and fuel consumption in passenger vehicles.

For downsized engines to be comparable to their larger counterparts, the specific output performance must be increased by a ratio equal to the reduction in engine size. Turbocharging seems to be the most acceptable solution to meeting the requirements, with high pressure ratios achievable and well documented improvements in efficiency [1-6].

Engines found in today's compact sized passenger vehicles are considered small, but are usually more than twice the capacity of the engine designed, developed and tested for this research. Furthermore, the technology needed to replace these larger engines with smaller capacity downsized units already exists. Applying turbocharger technology to smaller engines provides an economically viable solution in the near term to meet both the world's future powertrain and environmental requirements.

OBJECTIVES

Previous experiments and analysis [7] have found that the extent to which larger engines can be downsized while still maintaining equal performance is combustion limited. Other hurdles such as structural engine design and turbocharger integration were shown not to restrict engine performance for any odd firing configuration (≥ two cylinders). Hence, the objectives of this paper are to provide some insight into the relatively unknown combustion effects and limitations for smaller capacity downsized engines, and hence are as follows:

- Define and overcome combustion hurdles in smaller capacity downsized engines to reliably enable the performance limit to be extended to 25 bar BMEP.
- Define engine combustion operating limits and resulting compression ratios (CRs) for varying performance levels, corresponding to varying levels of downsizing for a reduced bore size small engine.
- Determine combustion parameters for a smaller capacity downsized engine over a range of manifold absolute pressures (MAP) up to 270 kPa, engine speeds exceeding 10,000 rev/min and CRs ranging from 9 to 13.

EXPERIMENTAL ENGINE

The test engine used in experiments was specifically designed and developed at the University of Melbourne. Motivation behind the engine design was to provide a platform to enable the investigation of high levels of turbocharging and downsizing in a small inline two cylinder engine. As no small OEM production engine could be adapted to evaluate this concept, a four valve, inline two cylinder engine was designed and constructed to withstand the high combustion and inertia forces associated with near 300 kPa MAP and engine speeds exceeding 10,000 rev/min.

The 0.43 L twin cylinder in-line arrangement featured double overhead camshafts and four valves per cylinder. Most of the engine components were specially cast or machined from billets. Provisions in the piston design allowed for CR variations, allowing combustion system optimization. Valve motion and exhaust manifold geometry were held constant after initial optimization through modeling and experiments. The conventional PFI fuel delivery system utilized 98-RON pump gasoline, with fuel specifications previously outlined [7, 8].

Table 1: Specifications for the UniMelb 'WATTARD' engine.

ENGINE	UniMelb 'WATTARD' (Prototype)
TYPE	In-line twin, 4 stroke SI, Liquid-cooled, Aluminum head/ barrel/ crankcase Integral clutch/ transmission
CAPACITY	0.43 L
BORE x STROKE	69 x 58 mm
FIRING ORDER	Unequal (0°, 180° CA)
COMPRESSION RATIO	9-13:1 with piston modification
COMBUSTION CHAMBER	Pent roof, central spark plug
VALVE ACTUATION	8-valve DOHC
VALVE TIMING	IVO: 24° BTDC, IVC: 72° ABDC EVO: 57° BBDC, EVC: 9° ATDC
INDUCTION	Garrett GT-12 turbocharger, EMS controlled internal wastegate, Intake flow restricted (Ø 20 mm) Non-intercooled
FUEL DELIVERY	Sequential multi-hole PFI
ENGINE MANAGEMENT	Motec M4 EMS, M&W Pro 12 CDI
FUEL	98-RON pump gasoline

Due to the engine's original design objectives, airflow and hence power were limited by an intake flow restriction positioned upstream of the compressor. Further in-depth detail concerning the test engine is documented [7], with general specifications given in Table 1. Figure 1 highlights a design image together with a sectional view of the engine design.

Figure 1: Design image of the turbocharged UniMelb 'WATTARD' engine together with a sectional view highlighting the barrel, cylinder head and reciprocating assembly.

EXPERIMENTAL ENGINE RESULTS

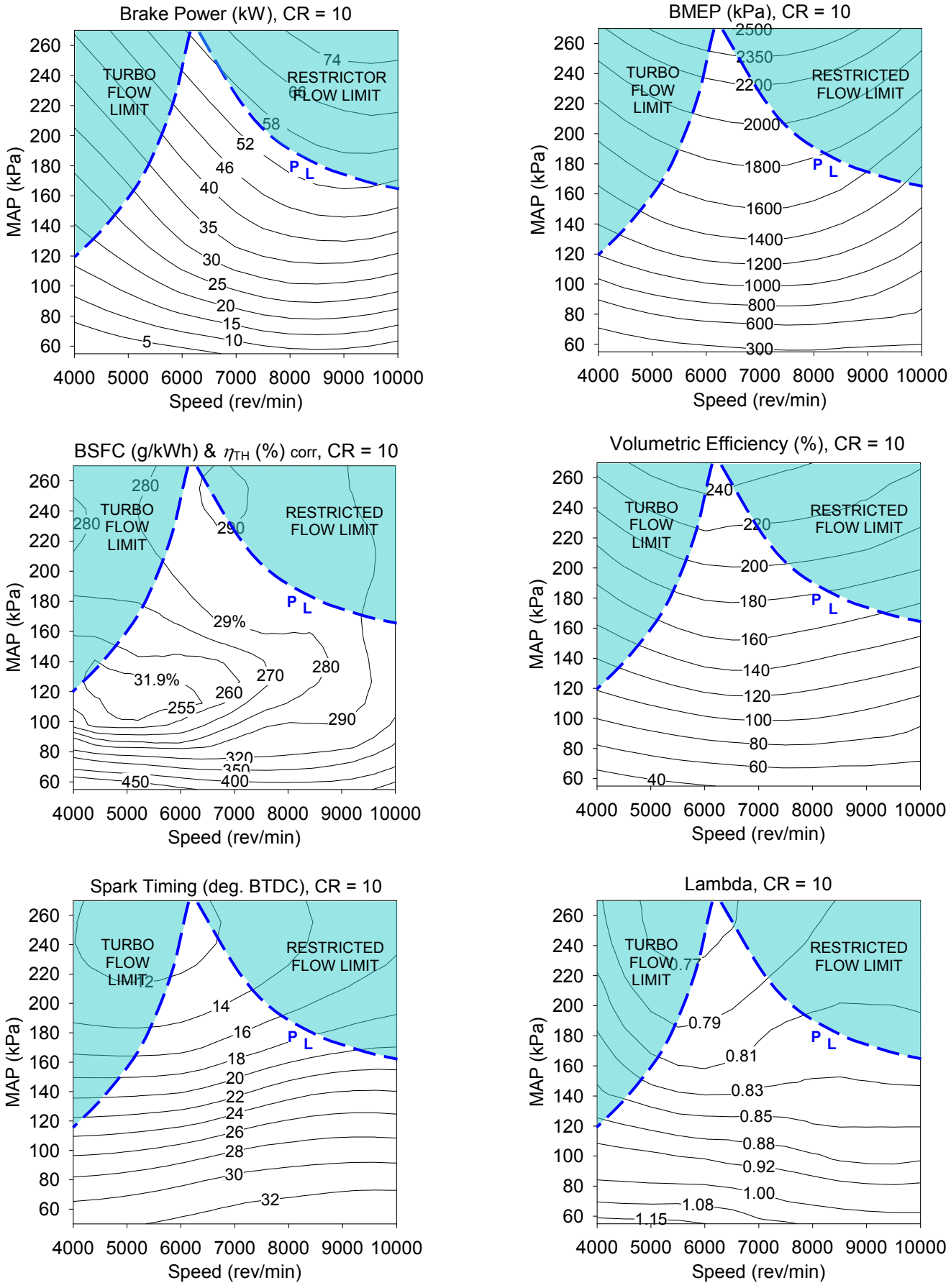

Figure 2: Turbocharged PFI experimental results for brake power, BMEP, BSFC, brake thermal efficiency (η_{TH}), volumetric efficiency, spark timing and lambda with varying engine speed and MAP parameters, CR=10. PL is the performance limit line defined at WOT. Airflow limit performance level *(25 bar $BMEP_{MAX}$)*.

To put the research into context, experimental engine results at the maximum specific output setting and associated CR of 10 are displayed in Figure 2, with further detail on the test engine previously published [7-13]. To reliably achieve 25 BMEP, the asymmetric (odd) fire configuration required the uneven flow conditions in the intake and exhaust systems to be accommodated in the engine design [12, 13]. In addition to the turbocharged results displayed in Figure 2, the test engine achieved a maximum of 37% brake thermal efficiency in normally aspirated configuration [7, 9]. However, this was only possible after CR optimization to compensate for the higher levels of dissociation, friction and heat losses associated with the smaller cylinder capacity.

Best engine performance, efficiency and CO_2 benefits across normally aspirated, supercharged and turbocharged modes were found to match or exceed the capabilities of typical larger bore engines found in passenger vehicles [7]. The case study performed determined the feasibility of replacing a 1.25 liter normally aspirated engine found in the 2007 Ford Fiesta with the development engine in the turbocharged mode [10]. Results show that the power and hence acceleration performance of the larger engine could be readily matched with the smaller turbocharged unit, with a 66% reduction in engine capacity. Simulated performance over the New European Drive Cycle showed a possible 22% reduction in fuel consumption and CO_2 emissions, including a reduction of 62% at idle conditions. These benefits are a consequence of operating the test engine closer to peak efficiency, together with engine and chassis mass reductions. The reduction in CO_2 would shift the study vehicle well under the 2012 Euro target of 120 g/km.

Across all modes, it was evident that the test engine (~70 mm bore) could operate with considerably higher CR for a given MAP when compared to larger bore (80-100 mm), lower speed engines. This was demonstrated with normally aspirated results showing potential for engine operation at a compression ratio exceeding 13 [9]. However, the dominant performance limiting factor was experimentally found to be abnormal combustion, specifically knock in the end-gas region, with the highest knock intensities deduced to occur on the intake side of the pent roof combustion chamber [7].

COMBUSTION SYSTEM DEVELOPMENT

Combustion system development is outlined, including mapping various CRs versus performance levels to define engine operating limits. Furthermore, implemented strategies to improve combustion stability at mid-high engine speeds and boost levels are described. As abnormal combustion is not the focus of this paper, abnormal combustion system development and combustion analysis surrounding this phenomenon are not described in this paper. Further detail on this topic relating to this research, including combustion insight into mega knock, is available [7].

COMPRESSION RATIO OPTIMISATION

Experimental testing included mapping various CRs versus performance levels to define engine operating limits. Performance levels included:

- 150 kPa MAP (wastegate limited), *16.5 bar $BMEP_{MAX}$*
- 200 kPa MAP (wastegate limited), *20 bar $BMEP_{MAX}$*
- Airflow limit (turbocharger, restrictor), *25 bar $BMEP_{MAX}$*

Testing commenced at the highest achievable CR with this piston design (Figure 3), corresponding to 13. When knock was encountered, the first stage of knock control relied on traditional tuning methods involving varying degrees of spark retard and/or fuel enrichment, albeit with the penalty of increased fuel consumption. If knock control could not be achieved through the EMS using these tuning strategies, the CR was then decreased in accordance with the knock severity, with performance levels subsequently retested at the reduced CR to find the limits of operation. Table 2 defines the knock limit (KL) and damage limit (DL) previously published by Rothe et al. [14], used to determine if CR reductions were needed to ensure engine reliability. The knock amplitude (KA) used to quantify limits [14], is defined as the zero to peak pressure of the high pass filtered (Butterworth) cylinder pressure (20 kHz sampling, 1.2 kHz cut-off frequency).

Table 2: Knock and damage limits previously defined by Rothe et al. [14] used to define engine operating limits.

Knock Amplitude (KA)	Zero to peak pressure of the filtered cylinder pressure
Knock Limit (KL)	1% of cycles with KA > 4 bar
Damage Limit (DL)	1% of cycles with KA > 20 bar

Figure 4 displays the knock and airflow limitations as functions of engine speed, MAP and CR. The cross plots have been constructed from multi-CR experimental data points. These CR values included 9.6, 10, 11, and 13. The resulting piston crown and combustion chamber shapes associated with each CR are displayed in Figure 3. It is noted that squish areas around the periphery of the chamber were maintained to minimize the variation in squish generated turbulence and vorticity, limiting any resulting combustion effects from varying CRs. However, changes to the turbulent length scale were inevitable due to the changes in the combustion chamber dish depth as the CR was altered.

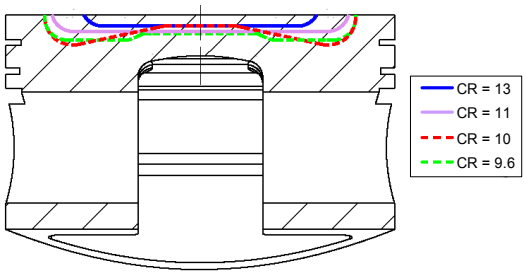

Figure 3: Piston sectional view illustrating the combustion chamber geometry for varying CRs. Combustion chamber geometry is symmetrical about the piston central axis.

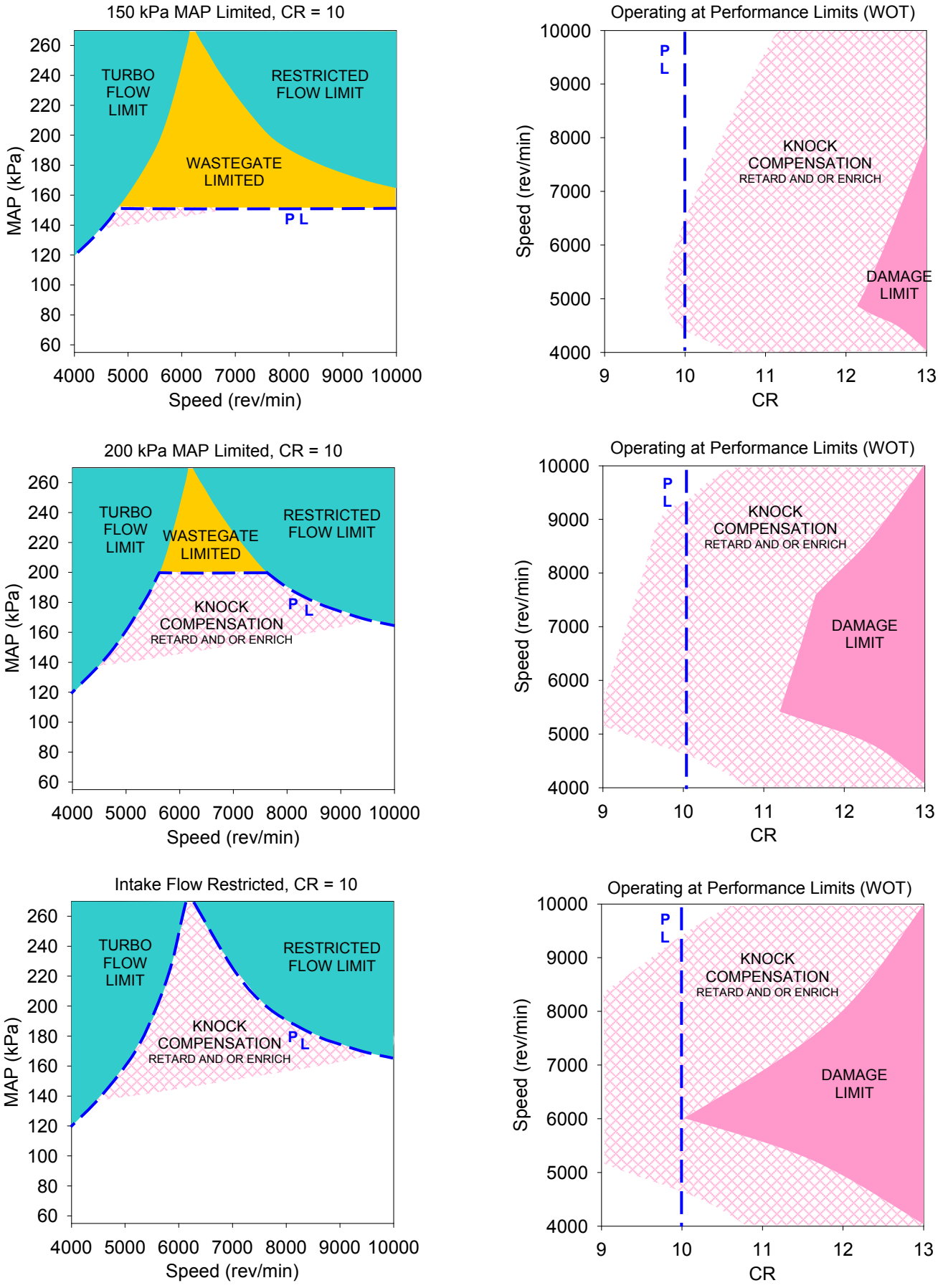

Figure 4: Knock and airflow limitations versus engine speed, MAP and CR. Cross hatched areas indicate operation with spark retard and/or fuel enrichment to compensate for knock. Shaded areas indicate non-operation due to knock levels above the damage limit or limited airflow. PL is the performance limit line at WOT for a given CR and MAP level. (Left): Engine speed versus MAP domain at CR =10. (Right): CR versus engine speed domain at the performance limit (WOT). (Upper): 150 kPa MAP limited, *16.5 bar* $BMEP_{MAX}$. (Middle): 200 kPa MAP limited, *20 bar* $BMEP_{MAX}$. (Lower): Airflow limit, *25 bar* $BMEP_{MAX}$.

The cross hatched areas in Figure 4 indicate domains where engine operation was knock limited but could be controlled via tuning strategies to avoid the damage limit. The shaded areas in plots indicate where engine operation was not possible due to airflow limitations or knock levels exceeding the damage limit. Airflow limitations were associated with insufficient compressor delivered airflow or a choked intake restriction. The performance limit (PL) is highlighted by the dashed blue line, corresponding to WOT for a given CR and MAP level.

With knock compensation tuning strategies (varying degrees of spark retard and/or fuel enrichment) together with CR reductions being the only forms of knock control used throughout experimentation, the cross plots displayed must first be put into context. It is noted that further knock reductions are expected with the implementation of various other strategies thus allowing increased MAP and/or CR before exceeding the damage limit. These strategies could include direct injection, cooled EGR, intake charge cooling (intercooling and/or evaporative), variable valve motion, combustion enhancement through chamber design and increases in fuel quality [1, 15-19]. However, these knock preventative strategies were not implemented during experiments due to their added complexity and as such were out of the scope of the project.

Table 3 summarizes CR results displayed in Figure 4, with the estimated highest useful compression ratio (HUCR) determined from the experimental data. Some safety margin was assumed in the estimation to ensure the damage limit was avoided.

Table 3: Estimated highest useful compression ratio (HUCR) from turbocharged experimental test data operating limits displayed in Figure 4, with some safety margin.

Performance Level	**HUCR**
150 kPa MAP *(16.5 bar $BMEP_{MAX}$)*	11.9
200 kPa MAP *(20 bar $BMEP_{MAX}$)*	10.9
Airflow limit @ 270 kPa MAP (*25 bar $BMEP_{MAX}$)*	9.8

Results from Figure 4 show that is advantageous to optimize the CR to a fixed value, resulting in incremental levels of rising MAP for engine speed increases to maximize power and efficiency, while continuously avoiding the damage limit. Furthermore, specific MAP levels are shown to define the HUCR. At 150 kPa MAP, the HUCR with some safety margin is shown to be 11.9 compared to 10.9 for the 200 kPa MAP case. These CR values are relatively high when compared to larger bore engines with similar boost levels [3, 20-22], mainly attributed to the reduced flame travel path to consume the last burning end-gas and the reduced end-gas volume around the periphery of the chamber.

Trends from Figure 4 confirm that for a given MAP and CR condition, the engine is less susceptible to knock at higher speeds [8, 10, 12, 13]. The reduced knock likelihood is a consequence of the increased flame speeds within the combustion chamber (Figure 9), which consume the unburned mass in the end-gas region more quickly. Increasing flame speed decreases the likelihood of knock due to the reduced end-gas residence time within the combustion chamber. It is also interesting to note that spark retard and/or fuel enrichment can be used as methods of knock control for up to 1-2 CR points depending on the knock severity. This can be a useful tool during boosted engine development, as it allows some safety margin to avoid the damage limit without having to reduce the CR. Moreover, this method of knock control allows the operating limit to be extended, thus enabling increased performance. However, the possible efficiency increases due to potential CR and/or MAP increases were found to be offset by the increased enrichment and less optimum spark timing.

The relationship between engine speed, MAP and CR parameters and their effect on the operating limits have been described for this small engine. Experiments highlighted that spark knock is the most dominant factor in limiting the performance of this small engine. However, reductions in end-gas knock severity at similar MAP and CR has enabled the performance operating limits to be extended for this particular small engine when compared to larger units. This is demonstrated with a peak BMEP value of 25 bar recorded at the airflow limit of 270 kPa MAP and a CR of 10. The increased performance of this small engine is attributed to the physical size reduction, particularly the reduced bore size (when compared to passenger vehicles) and the fast burn combustion chamber. This results in engine speed increases together with end-gas volume reductions around the periphery of the chamber, allowing CR and/or MAP values to be increased before exceeding the damage limit. This has major benefits in extending the operating limits in downsized applications.

IGNITION SYSTEM

The non-wasted spark ignition system included a two channel M&W Pro-12 capacitive discharge ignition (CDI) module connected to coil on plugs (COP) which was controlled by the EMS. The system required varying levels of ignition energy during combustion system development in order to optimize performance and fuel economy.

Before moving to boosted combustion, normally aspirated versions of the engine were developed with 50 mJ of ignition energy, in-line with conventional automotive vehicle ignition systems [23]. This system was adequate for normally aspirated testing, however for boosted operation, combustion stability worsened with increasing levels of boost as shown in the upper diagram of Figure 5. Troubleshooting methodology to improve combustion stability included EMS calibration changes and ignition system hardware replacement, with no improvements observed. Furthermore, various spark plug types and heat ranges were tested, with no improvements in combustion stability.

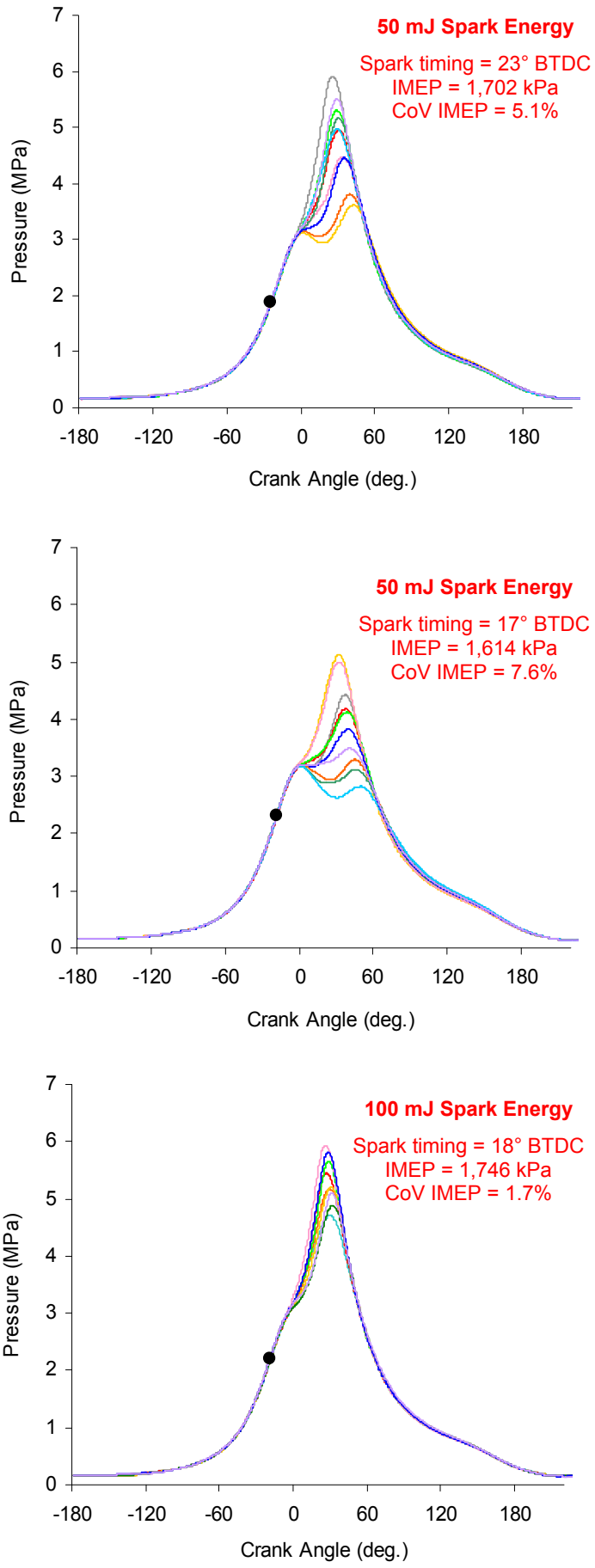

Figure 5: Turbocharged PFI consecutive tests displaying the effect of varying ignition energies over 10 consecutive cycles on boosted combustion. 6000 rev/min, 160 kPa MAP, CR = 10, lambda = 0.85 +/- 0.02.

Determining the minimum required ignition energy to provide stable combustion is an important parameter as the energy significantly affects the flame kernel initiation and hence growth. The initiation and growth significantly affect the combustion variability as the flame kernel needs to reach a radius of 10 mm before it can become fully independent of the spark energy [24-26]. At this stage, the flame kernel size is significant enough so that both large and small scale turbulence may distort the surface by wrinkling, thereby increasing the flame speed as it develops into a turbulent flame.

When compared to normally aspirated engines (even with high CRs), boosted engines require higher minimum spark energies due to the higher charge densities at the point of ignition. The primary impact on combustion from the increased ignition energy is the reduced flame development time due to the more rapid initial flame kernel growth. Hence, the higher ignition energy results in a larger flame kernel during the inflammation process, which thereby modestly reduces the MBT spark timing [16, 27-29]. Consequently, the ignition energy was an important parameter in the development of the high BMEP engine.

The combustion effects with varying ignition energies under mild boost conditions at 6,000 rev/min are displayed in Figure 5. At this speed with 160 kPa MAP and 50 mJ of spark energy, MBT spark timing with no knock mitigation strategy was 23° BTDC. However, for these conditions, at the optimum power mixture, combustion variability was large with 5.1% CoV of IMEP as shown in the upper diagram of Figure 5.

It is well known that as the charge density increases, more ignition energy is required [16, 30]. The flame kernel growth is influenced by the local flow including the turbulence intensity, the mixture composition (including residuals) and the gas temperature (all of which increase with increasing charge density). Under these high load conditions, the cyclic turbulence variations are the most probable cause of the combustion variability that occurs with the marginal ignition energy. The influence of the ignition delay is evidence of this, as represented by the 0-10% burn duration of 28° crank angle (CA) at these operating conditions.

Thus when the energy is doubled (Figure 5 - Lower), MBT spark timing reduces to 18° BTDC, the CoV of IMEP becomes more normal (1.7%) and the 0-10% burn duration reduces to 24° CA. The reduced combustion variability and increased initial burning rates are due to the more rapid flame kernel growth, with the rapid growth associated with the changing distorted wrinkled flame surface area. The middle diagram of Figure 5 displays the engine performance at 50 mJ of ignition energy with similar spark timing to the higher energy case shown in the lower diagram. Under these operating conditions with effectively retarded spark timing, the CoV of IMEP deteriorates (7.6%) and the 0-10% burn duration increases to 32° CA. Additionally, the IMEP falls by 7% from the MBT spark timing condition with this energy, whereas the IMEP increases by 4% for the increased ignition energy case at MBT spark timing.

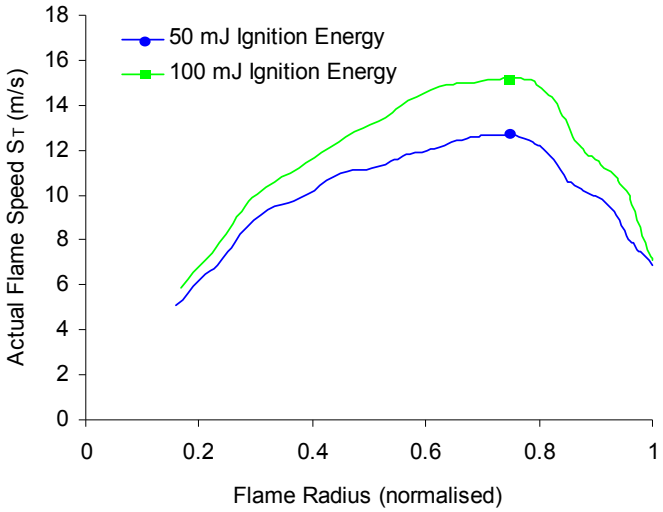

Figure 6: Turbocharged PFI consecutive tests displaying the effect of varying ignition energies on flame development. 6000 rev/min, 160 kPa MAP, CR = 10, 17 - 18° BTDC spark timing.

The flame growth for both ignition energies at similar spark timing is also compared in Figure 6, which highlights the improved kernel growth for the higher ignition energy case. The higher ignition energy has caused faster flame development which improves the turbulent flame speed as the flame radius expands to consume the charge. The overall 0-90% burn duration for the high energy ignition system under the conditions of Figure 5 is 48° CA (Figure 7). This is unusually small for engines of this capacity and even at 10,000 rev/min only increases to 59° CA, which is indicative of the high efficiency of the compact fast burn combustion chamber.

It should also be noted that the increase in ignition energy had no negative effect on the longevity of the 10mm spark plug over the life of the test program, with no visual signs of abnormal electrode wear. The most suitable spark plug type during development was found to be an iridium series with a 0.4 mm diameter tip. Varying spark plug heat ranges were utilized during development with the final heat range chosen to prevent fouling during cold ambient conditions but avoid plug overheating under high loads.

COMBUSTION ANALYSIS

Combustion analysis results are presented for the airflow limit performance setting of 25 bar BMEP, corresponding to a CR of 10. Combustion analysis was completed using E-CoBRA [31], an in-house two-zone quasi-dimensional model developed and validated by Hamori [32]. E-CoBRA was adapted to incorporate the modern four valve, pent roof geometry of the test engine. This involved the calculation of the flame area burnt gas volume amongst other parameters as a function of the flame radius in relation to the spark plug location. The software was then applied to the experimental cylinder pressure versus CA data (0.5° CA sampling), enabling combustion parameters to be estimated. A flush mounted air-cooled Kistler 601-B1 pressure transducer was used to measure in-cylinder pressure, with TDC alignment achieved by interpreting motored log pressure-volume data [33, 34].

Figures 7 to 11 display turbocharged combustion analysis results for varying engine speed and MAP operating conditions. The IMEP and CoV of IMEP are displayed in the upper diagrams of Figure 7. The CoV of IMEP trends indicate that the combustion variability begins to increase as the engine speed surpasses 6,000 rev/min. The increased CoV of IMEP above this speed in the non-knock compensated regions is caused by increases in retained residuals or internal EGR due to the higher exhaust back pressure associated with the poor turbine efficiencies. This is evident in Figure 12 (Appendix A), which displays the exhaust versus intake pressure and pumping work. Further detail regarding turbocharger matching and the interaction between the intake and exhaust for this engine is documented [7]. In some circumstances, small amounts of retained residuals can improve combustion stability, especially at the lower combustion temperatures [16, 35] associated with reduced loads. However, the reverse of this effect is seen here due to the already elevated temperatures associated with boost and high speed operation, which increase the levels of dissociation. Nevertheless, only a minor change in combustion variability is recorded with the increased retained residuals, with stability continuing to lie well within stable limits [32].

The CoV of IMEP also changes for rising MAP, increasing from 1-3% as the engine is operated in the knock limited regions. The increase is caused by two effects. The first involves the knock compensation strategies, consisting of increasing levels of spark retard and fuel enrichment. The spark retard and fuel enrichment affect the initial burn and flame kernel growth, which increases combustion variability [16] and decreases combustion efficiency (Figure 8). The second effect is the actual occurrence of knocking cycles as the knock compensation strategies only succeed in suppressing the knock below the damage limit at the elevated MAP (Figure 10). Nevertheless, the variation in combustion variability could be eliminated if knock could be controlled using other well documented proven techniques previously discussed [7, 10, 13].

The mass fraction burned (MFB) and mass fraction burned rate (MFBR) data is displayed in Figures 7 and 8. The 0-10% MFB duration (in CA degrees) decreases with rising MAP across all regions, even those which are heavily knock compensated. Initial burn effects associated with the rising boost pressure are also displayed graphically in Figure 8. The faster initial burn is caused by the higher mixture density, which improves the flame initiation and hence kernel growth. Furthermore, as the engine speed increases, the 0-10% MFB data shows identical trends when compared to the normally aspirated data [7, 9, 36] with increased CA durations over reduced time intervals. It is interesting to note that the increased retained residuals in the non-knock compensated regions above 6,000 rev/min, due to the higher backpressure previously described, slows the initial burn duration at high speeds as seen in the middle diagram of Figure 7. The retained residuals result in higher rates of dilution which increase the ignition delay [16, 37, 38] and hence extend the 0-10% burn duration.

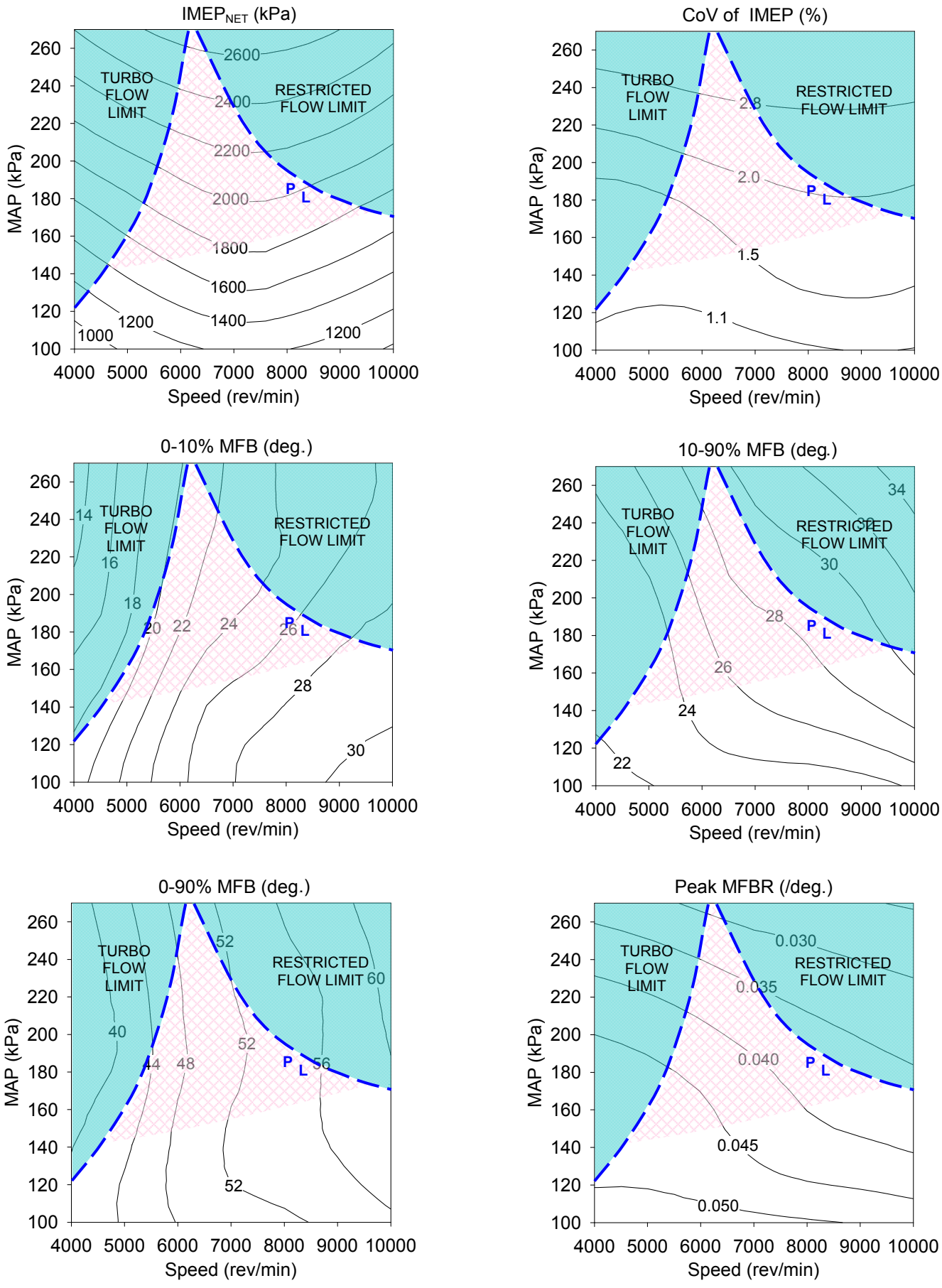

Figure 7: Turbocharged PFI combustion variability, mass fraction burned (MFB) and mass fraction burned rate (MFBR) effects for varying engine speed and MAP. CR = 10. Shaded areas = airflow limited regions. Cross hatched areas = knock compensated regions. PL is the performance limit line defined at WOT. Airflow limit performance level *(25 bar BMEP$_{MAX}$)*.

The 10-90% MFB (Figure 7) trends show increasing CA burn durations for rising MAP and engine speeds over the majority of the domain. This is unexpected as the increased charge density should promote faster burning rates due to laminar and hence turbulent flame speed increases. The reason for the increased burn durations is the retarded spark timing as the boost pressure increases, resulting in combustion deteriorations associated with slow burning cycles (Figure 8 - Lower). The reduced combustion efficiency associated with the retarded spark timing corresponds to the poor thermal efficiencies recorded as the boost pressure increases (Figure 2), despite the pumping losses reducing. Furthermore, there is a clear switch in the 10-90% MFB trend line directions in regions where there are high retained residuals or knock compensation. This is due to further reductions in combustion efficiency as the retained residuals decrease laminar flame speeds and hence slow the flame propagation.

The retarded spark timing promotes slow burning during the main energy release phase as indicated by the 10-90% burn duration data of Figure 7. This effect is offset by the faster initial burn (0-10% MFB), which results in no significant overall burn duration changes (0-90% MFB) over the majority of the test domain for rising MAP, as shown in Figure 7. However, minor 0-90% MFB changes are evident for MAP variation over a small part of the domain in regions that have higher rates of retained residuals. The dilution slows the initial and main phase energy release, resulting in an overall increase in burn durations over these regions. The 10-90% and 0-90% MFB data for engine speed variation follows identical normally aspirated trends [7, 9], with CA burn durations increasing with rising engine speed.

Hence, for boosted operation, faster overall burning which improves combustion and leads to thermal efficiency benefits can only be achieved if knock compensation strategies (non-optimal spark timing and fuel enrichment) are not heavily used. However, although these strategies reduce combustion efficiency and hence brake thermal efficiency, experimental results in Figures 2 and 4 have shown that the implementation of these knock control strategies have allowed for specific output increases via extending the MAP operating limits. Hence there is a tradeoff between peak power and good efficiency.

Figures 7 and 8 display the peak MFBR. It is noted that the MFBR is a normalized number allowing burn rate comparison over all operating conditions. However, actual mass burned rates (MBR) are dependent on the mass of charge consumed and thus increase with air consumption. The lower right diagram of Figure 7 shows that as the MAP increases, the peak MFBR decreases for reasons previously outlined describing the 10-90% MFB duration increases. This effect is clearly displayed at 7,000 rev/min in the lower diagram of Figure 8, with the retarded spark timing as the MAP increases from 100-180 kPa causing peak MFBR reductions, although the actual peak MBR increases by 60%.

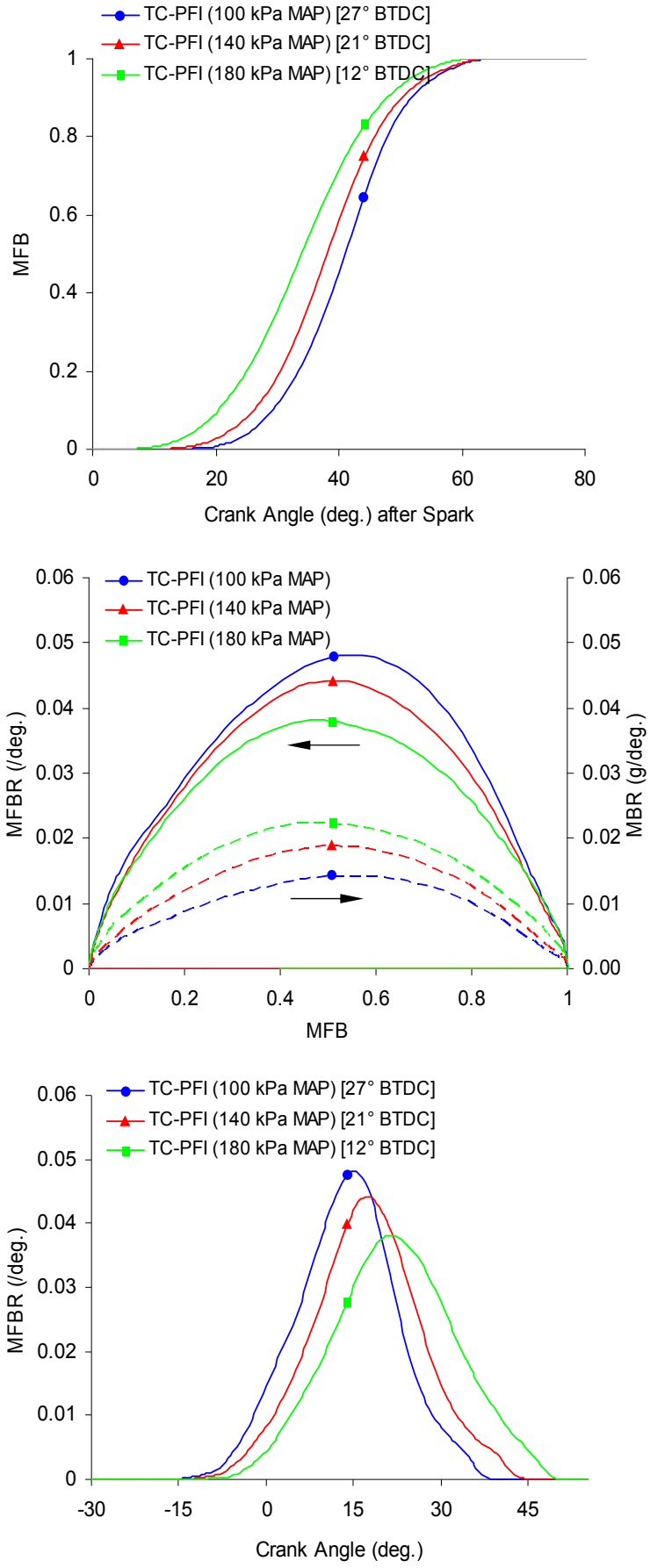

Figure 8: Turbocharged PFI combustion mass fraction burned (MFB), mass fraction burned rate (MFBR) and mass burned rate (MBR) effects for varying MAP. 7000 rev/min, CR = 10, spark timing [ ]. (Upper): MFB versus CA after Spark. (Middle): MFB versus MFBR (solid lines - left y axis) and MBR (dashed lines - right y axis). (Lower): MFBR versus CA.

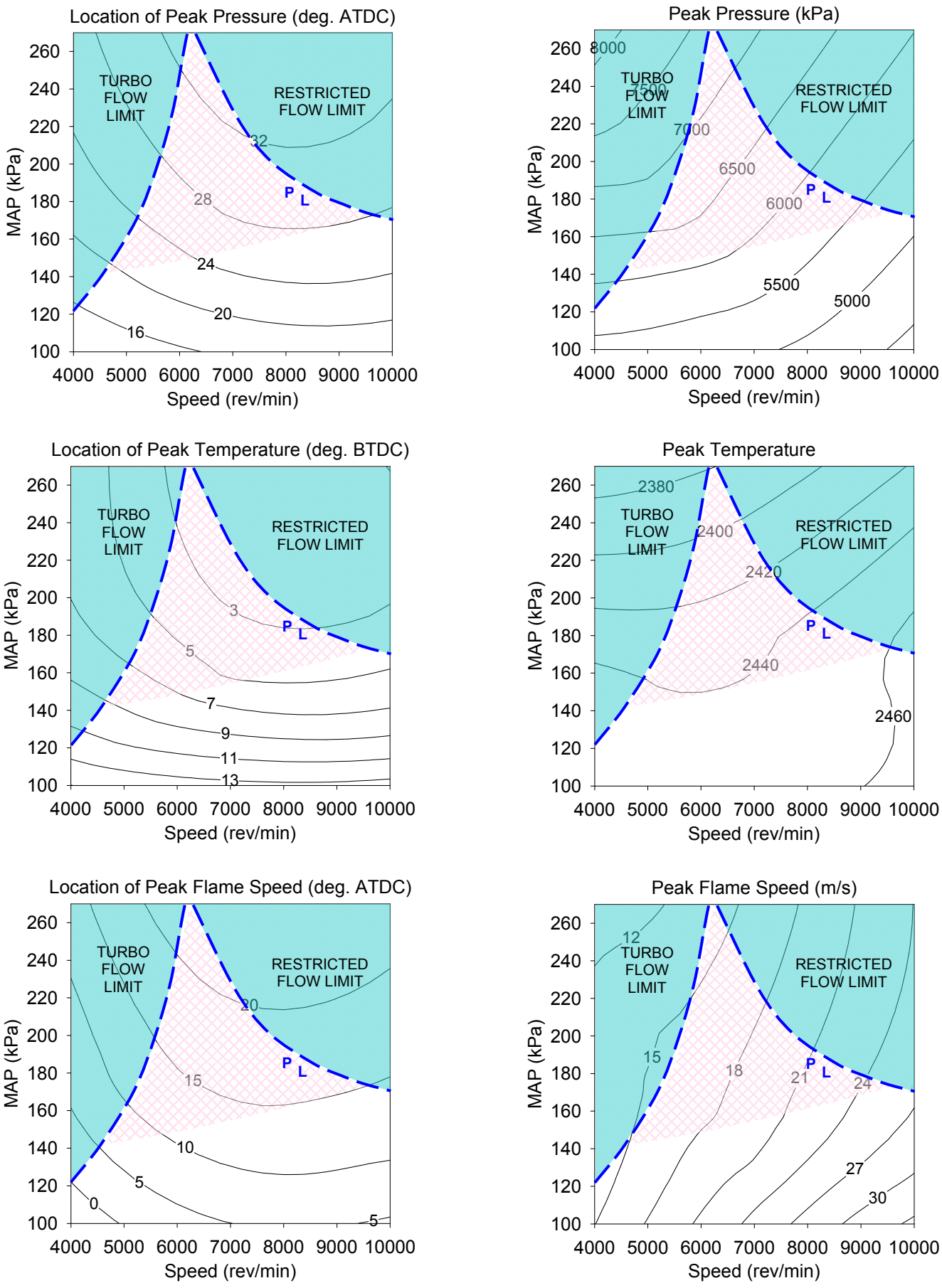

Figure 9: Turbocharged PFI combustion pressure, temperature and flame speed (actual turbulent flame speed with respect to the unburned gas velocity at the flame front) effects for varying engine speed and MAP. CR = 10. Shaded areas = airflow limited regions. Cross hatched areas = knock compensated regions. PL is the performance limit line defined at WOT. Airflow limit performance level *(25 bar $BMEP_{MAX}$)*.

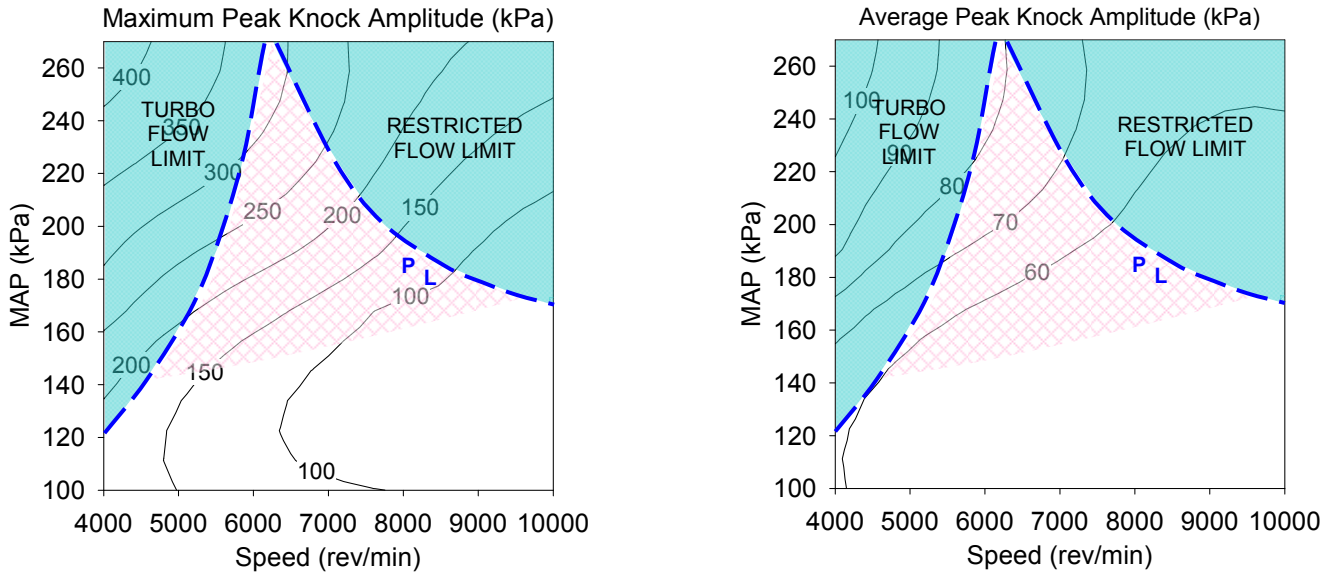

Figure 10: Turbocharged PFI combustion knock amplitude effects for varying engine speed and MAP. CR = 10. Shaded areas = airflow limited regions. Cross hatched areas = knock compensated regions. PL = performance limit line at WOT.

Figure 9 displays the peak pressure, temperature and flame speed effects. This data confirms the reduced combustion efficiencies when the MAP increases as previously described and shown in the MFB and MFBR data of Figures 7 and 8. The poorer main energy release burning profiles associated with the rising MAP, which is due to the retarded spark timing and increased retained residuals cause the peak temperature and hence flame speed to reduce, although the peak pressure continues to rise due to the higher charge density. This causes the peak pressure, temperature and flame speed locations to be further delayed in CA degrees.

Figure 10 presents maximum and average peak knock amplitudes. Both plots give identical trends, with the knock amplitude increasing in intensity as the boost pressure increases. The average peak knock amplitude indicates that combustion can be adequately controlled to avoid the upper knock limit of 4 bar previously defined. However, the maximum knock amplitude data shows that spark knock is not eliminated at high boost pressures, with the occasional cycle displaying some knocking tendency, although the pressure oscillations are minor and still below the defined damage limit of 20 bar. These results indicate that at high boost pressures, knock can not be completely eliminated, however it can be controlled to avoid engine damage.

Figure 10 also indicates that the knock intensity decreases with rising engine speeds due to flame speed increases (Figure 9) and reduced trapped charge above 6500 rev/min (Figure 2) for a given MAP. It is also noted that the retained residuals are higher at high engine speeds due to the increasing back pressure associated with the poor turbine efficiencies previously described, which may play a minor role in knock propensity reduction at elevated engine speeds.

Figure 11 displays turbocharged combustion effects at 50% MFB as the flame is fully developed allowing examination of the laminar and turbulent flame speeds. The upper diagrams display the 50% MFB CA location and MFBR. The 50% MFB position is shown to correspond to the previous temperature, pressure and flame speed location results displayed in Figure 9. These results all indicate later burning as the MAP is increased due to the retarded spark timing. The retarded spark timing also causes the MFBR to decrease at 50% MFB, although the actual MBR increases due to the increasing charge density. The decreasing MFBR for engine speed or MAP increases also corresponds to a reduction in burned gas temperatures at 50% MFB, which highlights the potential to reduce thermal NO_X emissions at high BMEP.

Figure 11 also displays the laminar and turbulent flame speed together with the turbulent to laminar flame speed ratio (FSR) at 50% MFB. The laminar flame speed for gasoline decreases with rising pressures and decreasing temperatures [39-41]. As previously shown in the normally aspirated combustion analysis [7], the laminar flame speed is largely unaffected by CR variation, also confirmed by Hamori [32]. However, as the MAP increases, the laminar flame speed at 50% MFB reduces due to the later combustion phasing (extension in the 50% MFB CA location or CA50) which reduces cycle temperatures. Although the cycle temperatures at 50% MFB decrease for rising MAP, the pressure continues to increase due to the improved charge density which enables improved power. The late-in-cycle main energy release phase due to the retarded spark timing causes the 10-90% burn duration to increase, which also results in the turbulent flame speed at 50% MFB to decrease for rising MAP. Although both the laminar and turbulent flame speeds reduce for rising MAP at 50% MFB, the turbulent to laminar flame speed ratio increases as shown in the lower diagram of Figure 11. For the rising MAP, the turbulent to laminar flame speed ratio increases as the laminar flame speed falls more rapidly than the turbulent flame speed, which is offset by increasing turbulence intensities that cause increased flame wrinkling and hence promote faster burning.

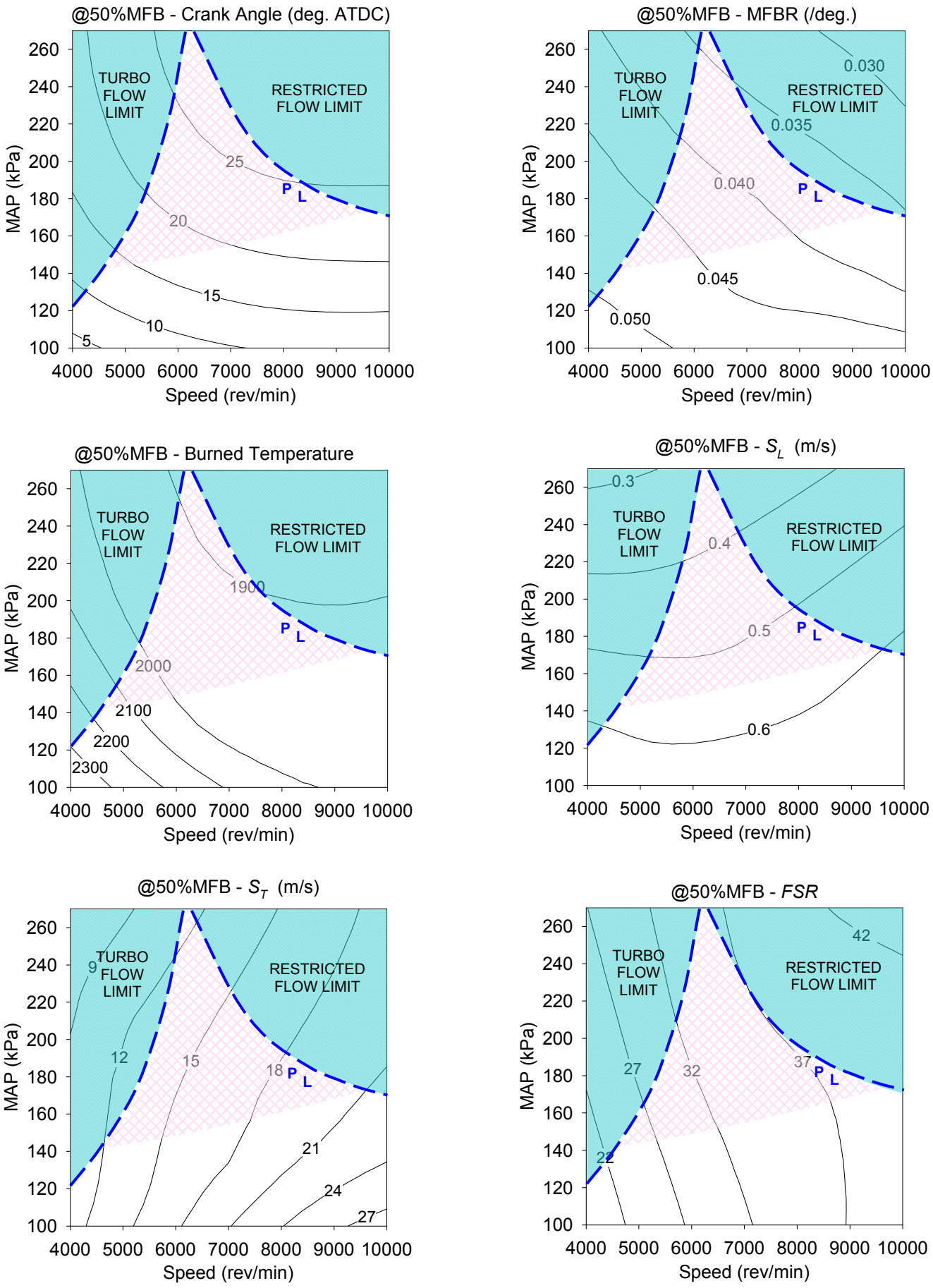

Figure 11: Turbocharged PFI combustion effects at 50% mass fraction burned (MFB) for varying engine speed and MAP. CA50 location, mass fraction burned rate (MFBR), temperature, laminar flame speed (S_L), actual turbulent flame speed (S_T) and turbulent to laminar flame speed ratio (FSR) displayed. CR = 10. Shaded areas = airflow limited regions. Cross hatched areas = knock compensated regions. PL is the performance limit line defined at WOT. Airflow limit performance level *(25 bar $BMEP_{MAX}$)*.

CONCLUSION

In this paper, combustion system development and combustion analysis results are presented for a 0.43 liter highly turbocharged PFI inline two cylinder engine. The effects of varying compression ratio, engine speed and manifold pressure on combustion were investigated for a highly downsized small engine, capable of reliably producing 25 bar BMEP.

Combustion system development involved mapping the small engine operating limits over varying performance levels (16.5, 20 and 25 bar BMEP), corresponding to varying levels of larger engine downsizing. Parametric variation included manifold absolute pressures up to 270 kPa, engine speeds exceeding 10,000 rev/min and compression ratios ranging from 9 to 13. Experiments highlighted that spark knock is the most dominant factor in limiting the performance of this small engine.

Best engine results at the airflow limit (25 bar BMEP) showed sustainable engine operation at the relatively high compression ratio of 10, which is significantly higher than that found in typical large bore engines at this operating condition. The increased performance of this particular small engine is attributed to the physical size reduction, specifically the reduced bore diameter (when compared to passenger vehicles) and the fast burn combustion chamber. This has major benefits in extending the operating limits in downsized applications.

Ignition system development highlighted the importance of flame kernel initiation and development in the combustion system of a highly boosted engine, where charge densities are significantly higher than normally aspirated powertrains. Doubling the ignition energy of a typical normally aspirated ignition system to 100 mJ of energy has resulted in significant improvements to combustion stability which has hence improved engine out performance, efficiency and emissions.

Combustion analysis was performed with in-house software, enabling the investigation of manifold pressure effects on combustion. Analysis illustrates that the increasing manifold pressure associated with intake boosting results in faster initial burn rates. However, the faster initial burn is offset by the slow main energy release which increases the 10-90% burn duration. The poorer combustion is associated with the retarded spark timing, which causes the peak temperature and hence flame speed to reduce, although the peak pressure continues to rise due to the higher charge density. Although the retarded spark timing causes the crank angle burn location to be further delayed for rising manifold pressure, the overall burn duration does not change.

The turbulent to laminar flame speed ratios were shown to increase for rising engine speeds and manifold pressure, despite decreasing turbulent flame speeds. However, the rate of laminar flame speed decline exceeded that of the turbulent flame speed resulting in increasing flame speed ratios. Peak values near 50 were recorded at engine speeds close to 10,000 rev/min.

The boosted combustion effects illustrate that the thermal efficiency is highly dependent on the combustion efficiency, which deteriorates rapidly if spark knock is encountered. Deterioration is associated with spark retard and/or fuel enrichment strategies which although suppress knock to extend the power limit, dramatically reduce combustion efficiency and hence brake thermal efficiency. This particular tuning strategy causes deterioration in three-way catalyst efficiency, however the vast majority of current vehicle powertrains do not operate at stoichiometric fueling under heavy load conditions. However, with this combustion system design strategy, potential drive cycle fuel consumption improvements in excess of 20% are still achievable.

ACKNOWLEDGMENTS

The authors are thankful to the numerous sponsors whose generosity made the UniMelb 'WATTARD' engine possible.

REFERENCES

1. Cairns, A., Blaxill, H., and Irlam, A., *Exhaust Gas Recirculation for Improved Part and Full Load Fuel Economy in a Turbocharged Gasoline Engine.* SAE Technical Paper Series (2006-01-0047), 2006.
2. Kleeberg, H., Tomazic, D., Lang, O., and Habermann, K., *Future Potential and Development Methods for High Output Turbocharged Direct Injected Gasoline Engines.* SAE Technical Paper Series (2006-01-0046), 2006.
3. Petitjean, D., Bermardini, L., Middlemass, C., and Shahed, S.M., *Advanced Gasoline Engine Turbocharging Technology for Fuel Economy Improvements.* SAE Technical Paper Series (2004-01-0988), 2004.
4. Rosenkranz, H.G., Watson, H.C., Bryce, W., and Lewis, A., *Drivability, Fuel Consumption and Emissions of 1.3 litre Turbocharged Spark Ignition Engine developed as a Replacement for a 2 litre Normally Aspirated Engine.* Proc. I.Mech.E., C 118/86: pp. 139-150, 1986.
5. Watson, H.C., Milkins, E.E., Roberts, K., and Bryce, W., *Turbocharging for Fuel Efficiency.* SAE Technical Paper Series (830014), 1983.
6. Arnold, S.D., Balis, C., Jeckel, D., Larcher, S., Uhl, P., and Shahed, S.M., *Advances in Turbocharging Technology and its Impact on Meeting Proposed California GHG Emission Regulations.* SAE Technical Paper Series (2005-01-1852), 2005.
7. Attard, W., *Small Engine Performance Limits - Turbocharging, Combustion or Design.* Thesis (Ph.D.), Department of Mechanical and Manufacturing Engineering, University of Melbourne, 2007. http://www.lib.unimelb.edu.au/eprints/ Accessed: 7 June, 2009.
8. Attard, W.P., Watson, H.C., Konidaris, S., and Khan, M.A., *Comparing the Performance and Limitations of a Downsized Formula SAE Engine*

in Normally Aspirated, Supercharged and Turbocharged Modes. SAE Technical Paper Series (2006-32-0072), 2006.

9. Attard, W.P., Konidaris, S., Hamori, F., Toulson, E., and Watson, H.C., *Compression Ratio Effects on Performance, Efficiency, Emissions and Combustion in a Carbureted and PFI Small Engine.* SAE Technical Paper Series (2007-01-3637), 2007.
10. Attard, W.P., Konidaris, S., Toulson, E., and Watson, H.C., *The Feasibility of Downsizing a 1.25 Liter Normally Aspirated Engine to a 0.43 Liter Highly Turbocharged Engine.* SAE Technical Paper Series (2007-24-0083), 2007.
11. Attard, W.P. and Watson, H.C., *Development of a 430 cm^3 Constant Power Engine for FSAE Competition.* SAE Technical Paper Series (2006-01-0745), 2006.
12. Attard, W.P., Watson, H.C., and Konidaris, S., *Highly Turbocharging a Restricted, Odd Fire, Two Cylinder Small Engine - Design, Lubrication, Tuning and Control.* SAE Technical Paper Series (2006-01-3637), 2006.
13. Attard, W.P., Watson, H.C., and Konidaris, S., *Highly Turbocharging a Flow Restricted Two Cylinder Small Engine - Turbocharger Development.* SAE Technical Paper Series (2007-01-1562), 2007.
14. Rothe, M., Heidenreich, T., Spicher, U., and Schubert, A., *Knock Behaviour of SI Engines: Thermodynamic Analysis of Knock Onset Locations and Knock Intensities.* SAE Technical Paper Series (2006-01-0225), 2006.
15. Gerty, M. and Heywood, J.B., *An Investigation of Gasoline Engine Knock Limited Performance and the Effects of Hydrogen Enhancement.* SAE Technical Paper Series (2006-01-0228), 2006.
16. Heywood, J.B., *Internal Combustion Engine Fundamentals.* McGraw-Hill, ISBN 0-07-100499-8, 1988.
17. Lake, T., Stokes, J., Murphy, R., Osborne, R., and Schamel, A., *Turbocharging Concepts for Downsized DI Gasoline Engines.* SAE Technical Paper Series (2004-01-0036), 2004.
18. Taylor, C.F., *The Internal Combustion Engine in Theory and Practice, Vol. 1 and 2.* The MIT Press, ISBN 0262700271, 1977.
19. SAE-International, *Traveling the Long Road to Gasoline Direct Injection.* Automotive Engineering International, SAE International Magazine, June Edition, 2006.
20. Edgar, J., *21st Century Performance.* Clockwork Media, ISBN 0-947216-90-1, 2000.
21. MacInnes, H., *Turbochargers.* HP Books, ISBN 0-912656-49-2, 1984.
22. Watson, H.C., Milkins, E.E., Roberts, K., Deslandes, J.V., and Bryce, W., *Turbocharging for the Fuel Efficient Urban Car.* SAE Japan, Proc. 2nd International Pacific Conference on Automotive Engineering, pp. 368-381, SAE Technical Paper Series (830192), 1983.
23. Dugdale, P.H., Rademacher, R.J., Price, B.R., Subhedar, J., and Duguay, R.L., *Ecotec 2.4l VVT: A Variant of General Motors Corporations Global 4-Cylinder Engine.* SAE Technical Paper Series (2005-01-1941), 2005.
24. Bradley, D., Hicks, R.A., Lawes, M., Sheppard, C.G.W., and Woolley, R., *The Measurement of Laminar Burning Velocities and Markstein Numbers for Isooctane-Air and Isooctane-n-Heptane-Air Mixtures at elevated Temperatures and Pressures in an Explosion Bomb.* Combustion and Flame, Vol. 115, pp. 126-144, 1998.
25. Gillespie, L., Lawes, M., Sheppard, C.G.W., and Woolley, R., *Aspects of Laminar and Turbulent Burning Velocity relevant to SI Engines.* SAE Technical Paper Series (2000-01-0192), 2000.
26. Lancaster, D.R., Krieger, R.B., Sorenson, S.C., and Hull, W.L., *Effects of Turbulence on Spark Ignition Engine Combustion.* SAE Technical Paper Series (760160), 1976.
27. Stone, R., *Introduction to Internal Combustion Engines.* Third Edition, Society of Automotive Engineers Inc., ISBN 0-7680-0495-0, 1999.
28. Song, J., Seo, Y., and Sunwoo, M., *Effects of Ignition Energy and System on Combustion Characteristics in a Constant Volume Combustion Chamber.* SAE Technical Paper Series (2000-05-0016), 2000.
29. Alger, T., Mangold, B., Mehta, D., and Roberts, C., *The Effect of Sparkplug Design on Initial Flame Kernel Development and Sparkplug Performance.* SAE Technical Paper Series (2006-01-0224), 2006.
30. Watson, H.C. and Andrews, G.E., *Road Transport Engine Emissions Course.* Lecture Notes, Department of Mechanical and Manufacturing Engineering, University of Melbourne, 2003.
31. Hamori, F., *Experimental Combustion Burn Rate Analysis (E-CoBRA).* Software, 2005.
32. Hamori, F., *Exploring the limits of Hydrogen Assisted Jet Ignition.* Thesis (Ph.D.), Department of Mechanical and Manufacturing Engineering, University of Melbourne, 2006.
33. Amann, C.A., *Cylinder Pressure Measurement and its use in Engine Research.* SAE Technical Paper Series (85206), 1985.
34. Lancaster, D.R., Krieger, R.B., and Lienesch, J.H., *Measurement and Analysis of Engine Pressure Data.* Engine Research Dept., General Motors Research Laboratories, SAE Technical Paper Series (750026), 1975.
35. Toulson, E., Watson, H.C., and Attard, W.P., *The Effects of Hot and Cool EGR with Hydrogen Assisted Jet Ignition.* SAE Technical Paper Series (2007-01-3627), 2007.
36. Attard, W.P., Toulson, E., Hamori, F., and Watson, H.C., *Combustion System Development and Analysis of a Carbureted and PFI Normally*

Aspirated Small Engine. SAE Technical Paper Series (2009-32-0188), 2009.

37. Quader, A.A., Kirwan, J.E., and Grieve, M.J., *Engine Performance and Emissions Near the Dilute Limit With Hydrogen Enrichment Using An On-Board Reforming Strategy.* SAE Technical Paper Series (2003-01-1356) 2003.
38. Lumsden, G., Eddleston, D., and Sykes, R., *Comparing Lean Burn and EGR.* SAE Technical Paper Series (970505), 1997.
39. James, E.H., *Laminar Burning Velocities of Isooctane-Air Mixtures - A Literature Review.* SAE Technical Paper Series (870170), 1987.
40. Muller, U.C., Bollig, M., and Peters, N., *Approximations for Burning Velocities and Markstein Numbers for Lean Hydrocarbon and Methanol Flames.* Combustion and Flame, Vol. 108, pp. 349-356, 1997.
41. Metghalchi, M. and Keck, J.C., *Burning Velocities of Air with Methanol, Isooctane, and Indolene at High Pressure and Temperature.* Combustion and Flame, Vol.48, pp. 191-210, 1982.

CONTACT

Dr. William Attard
Email: william_attard@hotmail.com

Prof. Harry Watson
Department of Mechanical Engineering
University of Melbourne
Victoria, Australia, 3010
Email: harrycw@unimelb.edu.au

DEFINITIONS, ACRONYMS, ABBREVIATIONS

ABDC	after bottom dead centre
ATDC	after top dead centre
BBDC	before bottom dead centre
BMEP	brake mean effective pressure
BSFC	brake specific fuel consumption
BTDC	before top dead centre
CA	crank angle
CDI	capacitive discharge ignition
CO_2	carbon dioxide
COP	coil on plug
CoV	coefficient of variation
CR	compression ratio
DOHC	double overhead camshafts
DL	damage limit
EGR	exhaust gas recirculation
EMS	engine management system
EVC	exhaust valve closed
EVO	exhaust valve open
FSR	flame speed ratio (turbulent to laminar)
HUCR	highest useful compression ratio
IMEP	indicated mean effective pressure
IVC	inlet valve closed
IVO	inlet valve open
KA	knock amplitude
KL	knock limit
L	liter
MAP	manifold absolute pressure
MBR	mass burned rate
MFB	mass fraction burned
MFBR	mass fraction burned rate
MBT	maximum brake torque
OEM	original equipment manufacturer
PFI	port fuel injection
PL	performance limit
PMEP	pumping mean effective pressure
RON	Research Octane Number
SI	spark ignition
S_L	laminar flame speed
S_T	actual turbulent flame speed (with respect to the unburned gas velocity at the flame front)
WOT	wide open throttle
η_{TH}	brake thermal efficiency

APPENDIX A

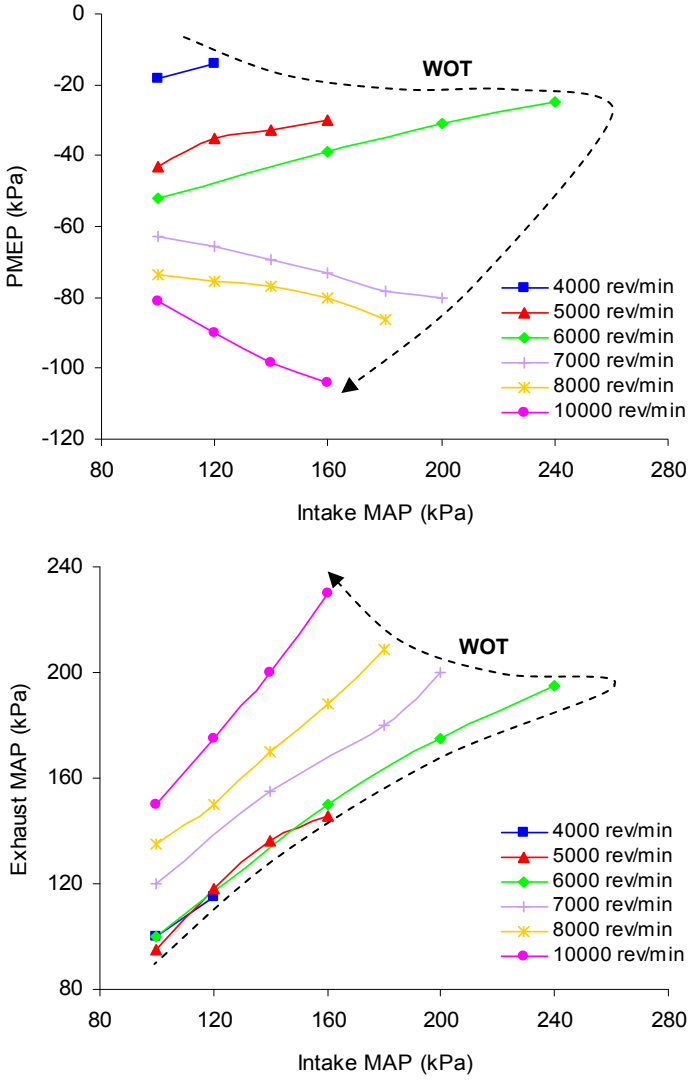

Figure 12: Turbocharged PFI intake and exhaust pressures and the effects on engine pumping work for varying engine speeds. CR = 10.

Author/s:
Attard, William P.; Toulson, Elisa; Hamori, Ferenc; Watson, Harry C.

Title:
Combustion system development and analysis of a downsized highly turbocharged PFI small engine

Date:
2009

Citation:
Attard, W. P., Toulson, E., Hamori, F., & Watson, H. C. (2009). Combustion system development and analysis of a downsized highly turbocharged PFI small engine. In SETC 2009: 15th Small Engine Technology Conference, Penang, Malaysia.

Publication Status:
In Press

Persistent Link:
http://hdl.handle.net/11343/26756

File Description:
Combustion system development and analysis of a downsized highly turbocharged PFI small engine